An Efficient Ultrasound Assisted Electrospinning Synthesis of a Novel Biodegradable Polymeric Ni-MOF Supported by PVA- Fibrous Network as an Efficient CH4 Adsorbent

Taher Shahriari
Birjand University of Medical Sciences
Narendra Pal Singh Chauhan
Bhupal Nobles' Sansthan
Ghasem Sargazi (g.sargazi@gmail.com)
Shahid Bahonar University of Kerman https://orcid.org/0000-0001-7340-0943
Ahmad Ebrahimi
Tehran University: University of Tehran
Alireza Hosseinzadeh
Tehran University: University of Tehran

Research Article

Keywords: Ni-MOF, Ultrasound irradiation, Electrospinning, Fibrous network, Adsorption, methane

Posted Date: November 11th, 2021

DOI: https://doi.org/10.21203/rs.3.rs-1058002/v1

An efficient ultrasound assisted electrospinning synthesis of a novel biodegradable polymeric Ni-MOF supported by PVA-fibrous network as an efficient CH_4 adsorbent

Taher Shahriari[a], Narendra Pal Singh Chauhan[b],*, Ghasem Sargazi[c],**, Ahmad ebrahimi[d] and Alireza Hosseinzadeh[d]

[a] Department of Environmental Health Engineering, Birjand University of Medical Sciences, Birjand, Iran

[b] Department of Chemistry, Faculty of Science, Bhupal Nobles' University, Udaipur-313002, Rajasthan, India.

[c] Noncommunicable Diseases Research Center, Bam University of Medical Sciences, Bam, Iran.

[d] School of Chemistry, College of Science, University of Tehran, Tehran, Iran

**Correspondence to E-mail: G. Sargazi (g.sargazi@gmail.com)

*Co-correspondence to E-mail: N. P. S. Chauhan (narendrapalsingh14@gmail.com, narenpolymer@gmail.com)

Abstract

In this study, Ni-MOF was synthesized via ultrasound irradiation under optimal conditions, which included an ultrasound power of 370 W, time duration of 20 minutes, and a temperature of 25 ^{o}C. The final Ni-MOF nanostructures were immobilized in PVA fibrous polymeric network using under optimal conditions (concentration: 8 wt %; the nozzle tip with flow rates of 0.10 mL/h; temperature: 25 ^{o}C and humidity: 22 %; voltages: 20 kV; spinning distance: 12 cm) of electrospinning. To characterize the final composition, various analyses were used. The presence of functional groups in structures was confirmed by FTIR. The Ni-MOF sample was uniformly synthesized on the surface of PVA, as evidenced by SEM and Mapping elemental analysis. The BJH technique validated the effect of the substrate's role in increasing the surface area of the final products. The final products of the Ni-MOF/PVA fibrous network were used as a novel adsorbent in the adsorption of CH_4 gas.

Keyword: Ni-MOF, Ultrasound irradiation, Electrospinning, Fibrous network, Adsorption, methane

1. Introduction

Metal organic framework (MOF) nanostructures are crystalline compounds made up of various metals and ligands [1, 2] . These nanostructures have received a lot of attention because of their remarkable properties like high specific surface area, significant porosity, low density, and excellent chemical stability [3]. These distinct properties have led to a wide range of applications for these compounds in fields as diverse as engineering [4], medicine [5], and energy storage [6] .

MOF nanostructures have been produced using a variety of methods, including hydrothermal, solvothermal, sol-gel, and electrochemical methods [7, 8]. According to our findings, the use of fast, controllable, and simple ultrasound methods has received more attention than conventional methods [9]. Through a biocompatible and biodegradable process, this effective method can control the properties of the final products.[10, 11] As a result, the use of a suitable synthesis method influenced the advancement of these nanostructures' applications [12].

Various procedures, such as the formation of composite structures, crystal nucleus and the formation of stable shapes on various substrates, have been used to improve the properties of MOF nanostructures [13]. Although these procedures improved the properties of final structures, the economic cost-effectiveness and non-uniform morphology of the samples reduced the samples' efficiency [14].

Polymeric nanostructures have desirable mechanical and physicochemical properties, such as a high surface area and significant porosity, which allows pollutant agents to make effective contact with highly assessable adsorption/desorption sites [15]. These nanostructures are used for a variety of applications, including environmental procedures, due to their distinguishing characteristics [16].

Combining the properties of MOFs and nanofibers can result in a novel protocol for designing new structures with highly efficient features that can be used in a variety of applications [18]. According to our findings, no research has been done on the use of Ni-MOF immobilized on the surface of PVA polymeric nanofibers.

Today, the amount of pollutants has increased significantly as industrial activity in world. Because of their floating properties, gaseous pollutants are much more prevalent among these pollutants [19]. CH_4 is one of the toxic gases, even in trace amounts causing serious environmental problems. As a result, the adsorption of this contaminant by novel nanostructures with high specific surface area and stability, as well as systematic studies to investigate the effect of effective parameters on CH_4 adsorption, is critical [20, 21].

In the present study, the Ni-MOF was synthesized for the first time by ultrasound irradiation. The final productions were immobilized in PVA-polymeric matrix, and characterized by relevant analysis of thermogravimetric analysis (TGA), derivative thermogravimetric (DTG), X-ray diffraction (XRD), scanning electron microscopy (SEM), Fourier transform infrared (FT-IR) spectroscopy, SEM, TG-DTG, energy dispersive spectrometer (EDS) elemental mapping images and BJH surface area techniques. The final products were used as a novel adsorbent for CH_4 adsorption. Finally, a fractional factorial design was used to conduct a systematic study of the effect of synthesis parameters on different product properties.

2. Experimental section

2.1. Materials and instrumentation

$Ni(NO_3)_3$ (Merck, 98%), pyridine-2,6 dicarboxylic acid (Merck, 99%) and acetic acid (Merck) were analytical grade. Polyvinyl alcohol (PVA) was purchased from Merck as an analytical grade reagent, and different solutions were prepared using double distilled deionized water.

The crystalline nature of the synthesized Ni-MOF nanostructures was determined using XRD with Cu K radiation (λ = 1.54 Å). Nitrogen adsorption/desorption measurements were carried out on a TriStar II 3020 analyzer at 77 K. The total surface area is calculated according to the BET equation. Surface morphology and particle size distribution are investigated using a field emission scanning electron microscope (SEM, Nova Nano SEM 230) equipped with an energy dispersive spectrometer (EDS). Fourier transform spectrometry was performed on a Nicolet-6700 FTIR spectrometer with a wavenumber range of 400–4100 cm^{-1}.

2.2 Synthesis of Ni-MOF samples

In a typical ultrasound synthesis, a solution of $Ni(NO_3)_3$ (0.0716 g, 0.2 mmol) and pyridine-2,6 dicarboxylic acid (0.1003 g, 0.6 mmol) was dissolved in 50 mL double-distilled water. The resulting solution was then stirred for approximately 30 minutes at 70 °C. The nanostructures were then placed in the ultrasound reactor under optimal conditions, which included a ultrasound power of 370 W, time duration of 20 minutes and a temperature of 25 ^{o}C. After 50 minutes, the white crystals were isolated by repeated centrifugation and washed with acetic acid several times to remove the excess reagents.

2.3 Synthesis of Ni-MOF/PVA fibrous network

For a typical ultrasound assisted electrospinning synthesis, a mixture of 10 mg Ni-MOF and 0.05 g PVA powder was dissolved in 8 mL acetic acid. The resultant solution was electrospinned under environment conditions (temperature: 25 ^{o}C and humidity: 22 %). The electrospinning conditions were optimized at 20 kV voltages and a spinning distance of 12 cm. Flow rates of 0.10 mL/h were used to eject the solutions from the nozzle tip, and the Ni-MOF concentration was set at 8% by weight. The proposed structure of Ni-MOF/PVA is shown in Scheme 1.

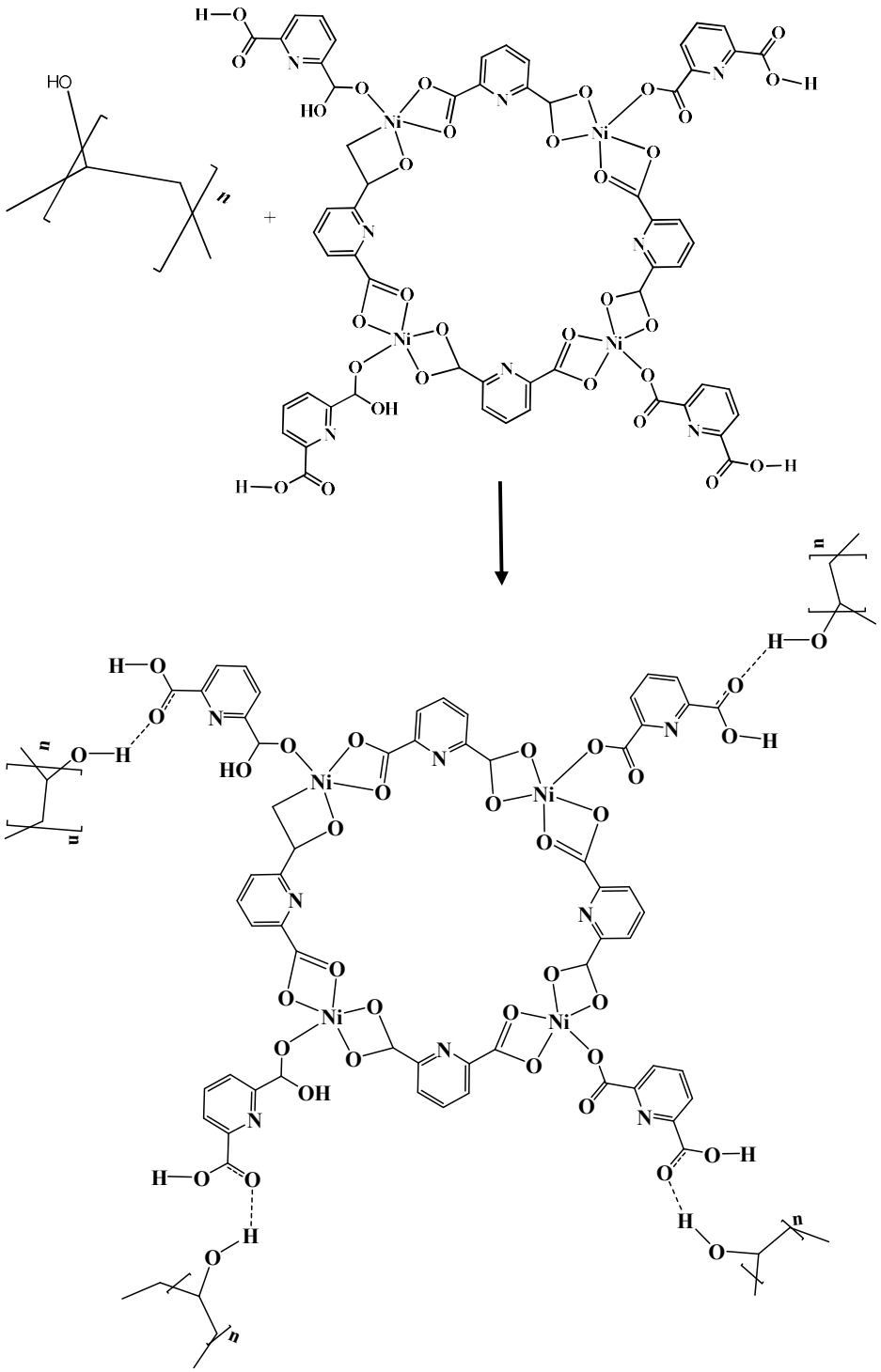

Scheme 1. The proposed structure for Ni-MOF/PVA electrospun nanofibrous membrane.

2.4 CH_4 gas adsorption procedure

An adsorption reactor was used to assess the amount of CH_4 adsorption by Ni-MOF nanostructures supported on PVA fibrous (Fig. 1). Where, P, N, R, T, and Z represent gas pressure, number of gas moles, and general constant of gases, equilibrium temperature, and compressibility coefficient in dozer, respectively. In next step, the adsorption gas moles were determined as follow: $n_{ADS} = n_1\text{-}n_2$. The compressibility parameters (Z_1, Z_2) was calculated according to methodology of our previous study [22].

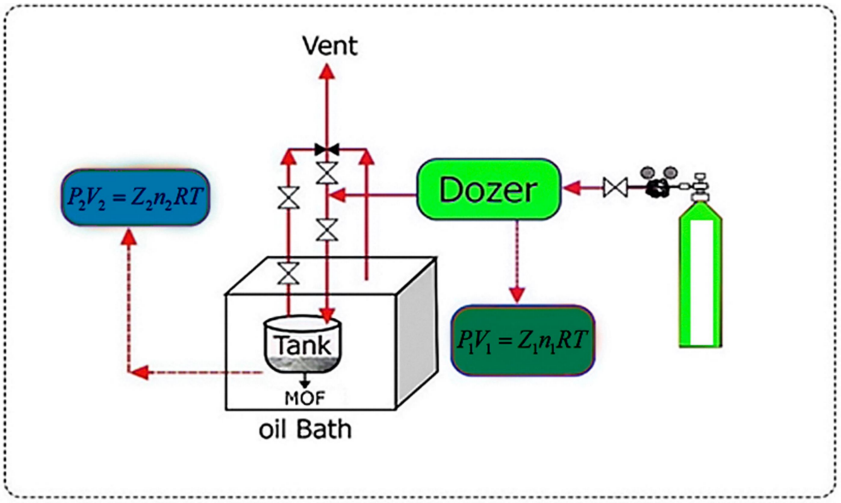

Fig. 1. Schematic procedure for voltametric setup for CH_4 gas adsorption.

2.5. Experimental design

Nanostructures have been considered as a novel candidate for CH_4 gas adsorption due to improved physiochemical properties such as high surface area, small size distribution and thermal stability. In order to obtain the optimal parameters, a factorial experiment design was used. The data included adsorbent dosage (***A***), temperature (***B***) and pressure (***C***). Considering these experimental parameters, 18 runs were selected, and the results with two replicates were exhibited in Table 2.

Table 1:

Coded and uncoded levels of adsorbent dosage, temperature and pressure for fractional factorial design.

Level	**Coded level**	**Uncoded level**		
		Temperature (°C)	Pressure (bar)	Dosage (mg)
Low	+1	20	1	10
Center	0	25	1.5	15
High	-1	30	2	20
Coded formula: $\frac{x-\frac{x\,(high)+x(low)}{2}}{\frac{x(\,high)-x(low)}{2}}$	**, x: -ω …, -3, -2, -1, 0, 1, 2, 3, …. +ω**			

Table 2: Randomized complete fractional factorial design for CH_4 gas adsorption experiments of Ni-MOF/PVA fibrous network.

Sample (Level)	Std order	Center Pt	A (mg)	B (°C)	C (bar)	REP	CH_4 Adsorption (mmol/g)
a	9	1	-1	+1	-1	1	1.9
						2	1.9
b	5	1	-1	0	-1	1	2.5
						2	2.5
c	6	1	0	-1	+1	1	3.0
						2	3.1
d	3	1	+1	0	0	1	2.5
						2	2.5
e	2	0	+1	-1	+1	1	2.6
						2	2.6

3.0 Results and discussion

3.1. FTIR spectrum

The FTIR spectra for Ni-MOF and Ni-MOF/PVA are depicted in Fig 2A and 2B, respectively. The coordinated water in the structures may be assigned to the absorption bands near 3450.5 cm^{-1} in both samples. The C-H group is associated with the frequency at 3075.8 cm^{-1}. The presence of a 2, 6 pyridine dicarboxylic acid ligand was confirmed by the presence of bands near 1651.7 cm^{-1}. The asymmetric C-N bonds are responsible for the bands observed at 1334.2 cm^{-1}. All corresponding absorption bands related to pure Ni-MOF are observed in Fig. 2B, which shows the FT-IR spectrum of Ni-MOF/ PVA nanofibrous composite, confirming the presence of Ni-MOF in the final structures.

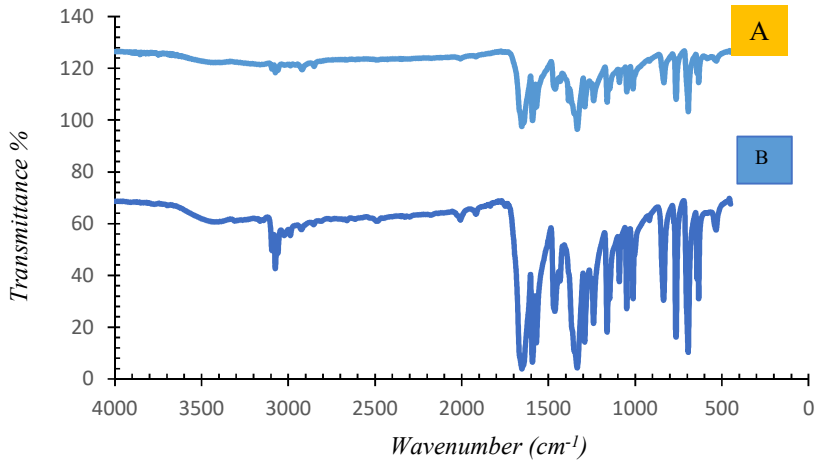

Fig. 2. FTIR spectra of (A) Ni-MOF prepared by ultrasound and (B) Ni-MOF/ PVA fibrous samples manufactured ultrasound assisted electrospinning method.

3.2 XRD patterns

XRD patterns of Ni-MOF synthesized under optimal ultrasound conditions and Ni-MOF/PVA fibrous networks were shown in Fig. 3. The peaks associated with the Ni-MOFs patterns with the cubic crystalline plate are well represented in the final structure based on these patterns. The crystallites are 18 nm in size, according to Debye Scherrer ($D=0.9\ \lambda/\beta \cos\theta$). In addition, the XRD patterns of Ni-MOF can be seen in the final structure of Ni-MOF/PVA fibrous networks, as shown in Fig. 3B, which is evidence of a successful nanosynthesis. Furthermore, according to the Debye Scherrer relation, the size of the crystallite in pure Ni-MOF is 34 nm, whereas it is 18 nm in the final structure of Ni-MOF/PVA, and this decrease in crystallite diameter can be attributed to the ultrasonic assisted electrospinning effects [23].

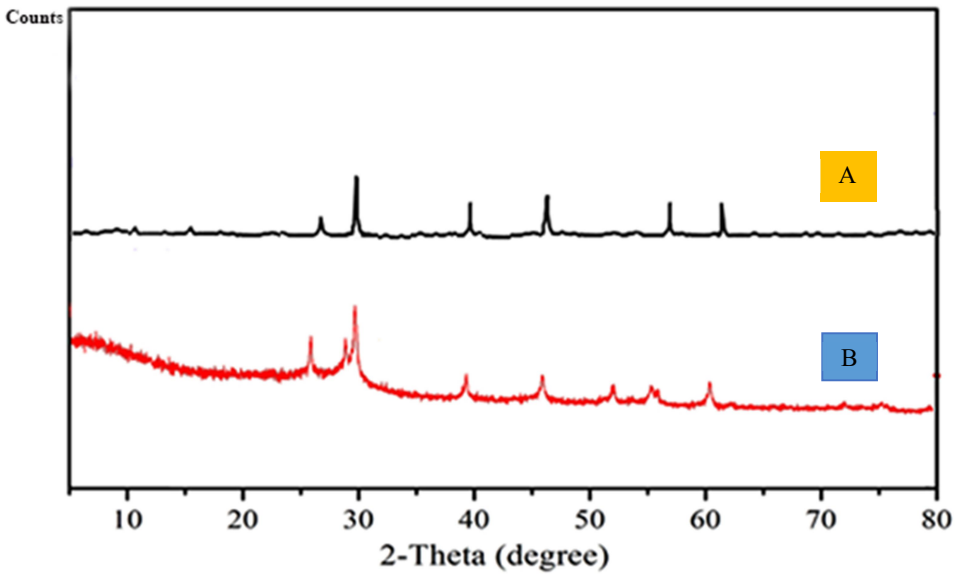

Fig. 3. XRD patterns of (A) Ni-MOF and (B) Ni-MOF/PVA fibrous networks.

3.3 Thermal behavior

The TG-DTG spectra of nanostructures are depicted in Fig. 4. Thermal stability of Ni-MOF and Ni-MOF/PVA structures are between 350 and 370 °C, according to the TG-DTG curve. The use of substrate, as is well known, improves the final product's stability. According to research, the thermal stability of the samples has increased significantly when compared to previous adsorbents [24]. However, due to the importance of thermal stability, the sample synthesized in this study is remarkable in terms of adsorption. Weight loss occurs in the following steps for both samples, which can be attributed to the collapse of the structure's components.

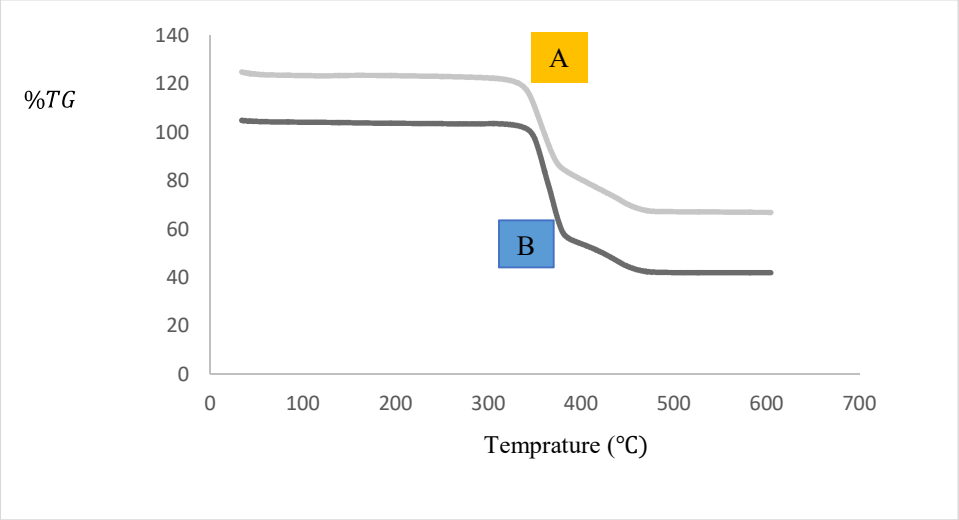

Fig. 4. Thermal stability of (A) Ni-MOF and (B) Ni-MOF/PVA.

3.4 SEM-EDX study:

The SEM images of (A) Ni-MOF and (B) Ni-MOF/PVA are shown in Fig. 5. The initial nucleation process of Ni-MOF can be seen clearly in Fig. 5 A. In addition, the morphology of the sample was changed to a fibrous network, as shown in Fig 5 B. As a result, there is no evidence of agglomeration in the final Ni-MOF/PVA structures. It is due to the optimal conditions of the electrospinning method [25]. Fig. 6 depicts the EDX spectrum for Ni-MOF/PVA. Table 3 also includes a summary of the elemental analysis using EDX. The empirical formula for Ni-MOF/PVA is $C_7H_{50}O_4Ni$. These analyses confirmed the presence of related elements in the final structure of Ni-MOF/PVA samples.

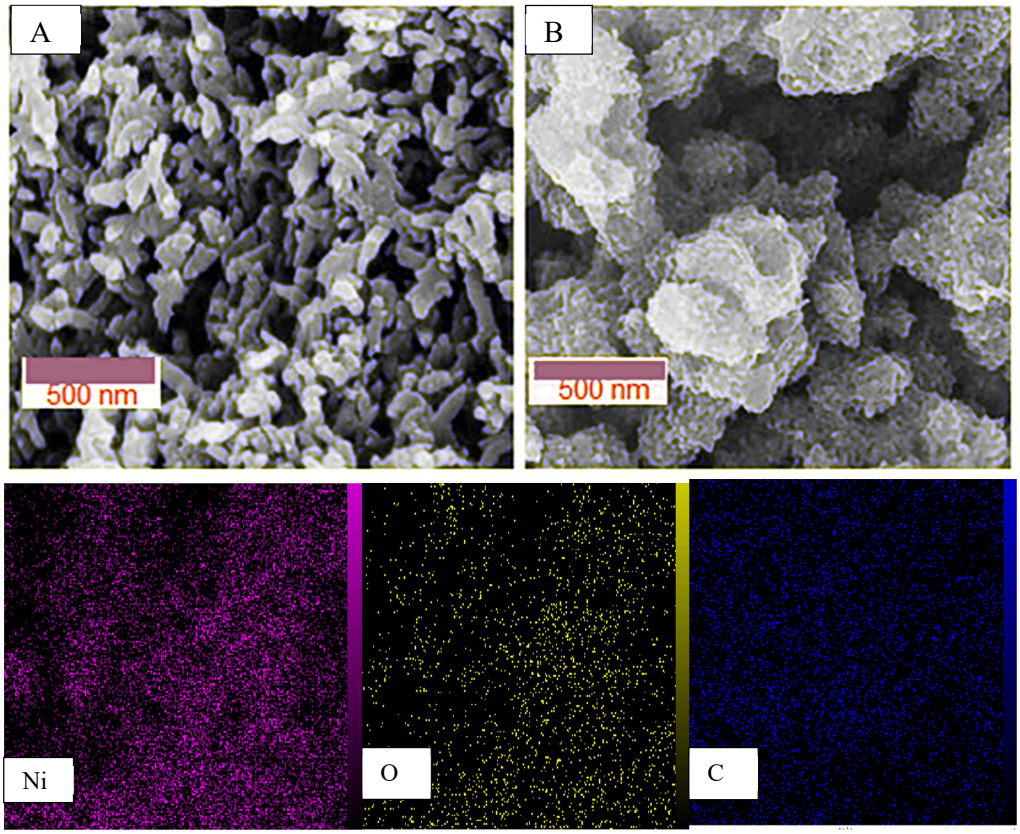

Fig. 5: SEM images for (A) Ni-MOF and (B) Ni-MOF/PVA and its mapping.

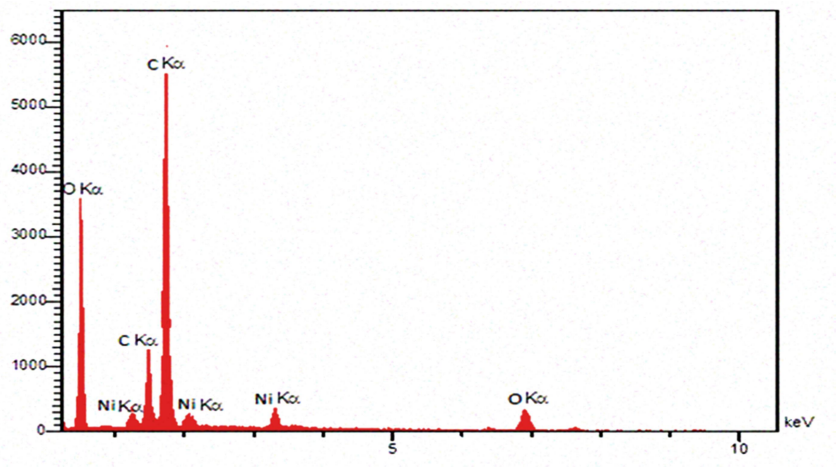

Fig. 6: EDX spectrum of Ni-MOF/PVA.

Table 3: Elemental analysis of Ni-MOF/PVA.

Element	Line	K	Kr	Weight-%	Empirical Formula
O	K_α	0.4224	0.2479	26.38	$C_7H_{50}O_4Ni$
C	K_α	0.0040	0.0024	32.52	
Ni	K_α	0.1630	0.0957	22.16	

3.5 Adsorption/desorption isotherm:

The N_2 adsorption/desorption isotherm and BJH plot of Ni-MOF/PVA fibrous network are depicted in Figs. 7 and 8, and the results are tabulated in Table 4. According to data, the adsorption/desorption behaviour is similar to the fourth type of classical isotherm. Based on BJH plot, the sample has a microporous size distribution, which can be seen in Fig. 8. According to the results, the surface area of the Ni-MOF/PVA samples is significantly greater than that of the previous reported Ni-MOF [26, 27]. It can be concluded that ultrasound assisted electro spinning route and selection the novel nanostructures can be

affect the surface area of final products.

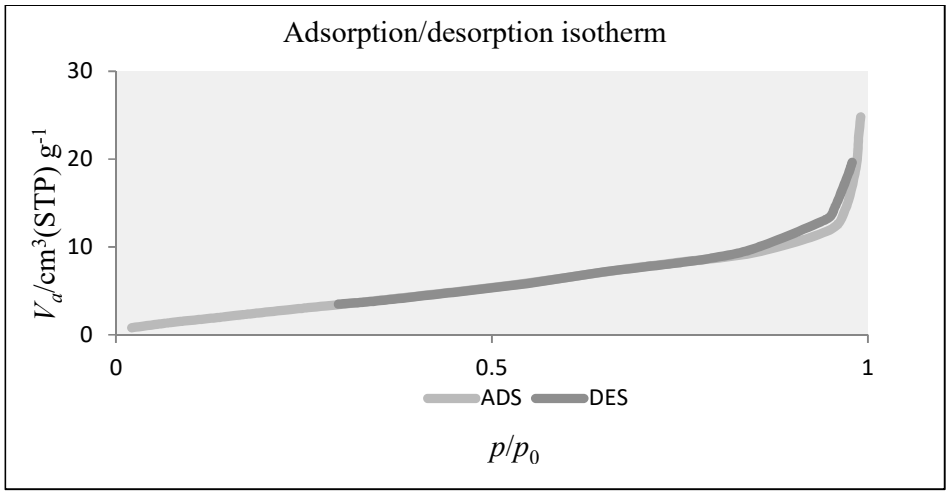

Fig. 7. Adsorption/desorption isotherms of Ni-MOF/ PVA samples

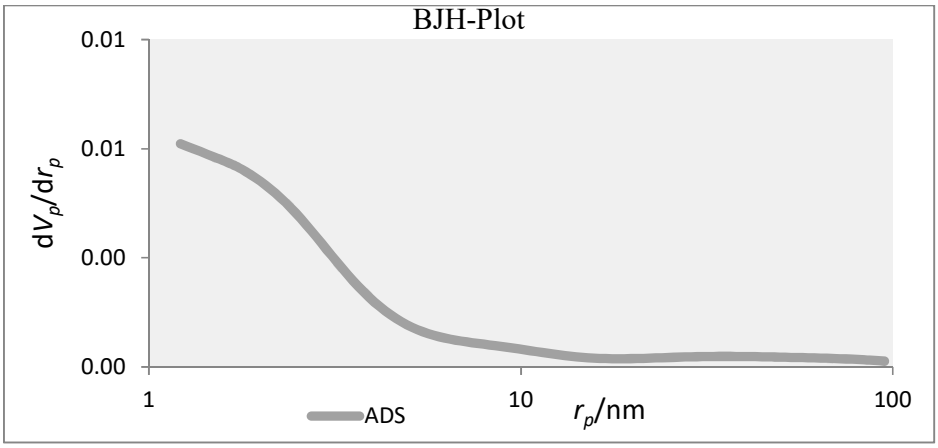

Fig.8. BJH plot for the pore size distribution of Ni-MOF/ PVA.

Table 4. BJH analysis data for Ni-MOF/ PVA.

Parameters	**Amount**
$V_{p\,(}cm^3\ g^{-1)}$	0.04
$r_{p,peak}$ (nm)	1.2
$a_{p\,(}m^2\ g^{-1})$	1840

3.5. Systematic study of procedure

Fig. 9 depicts a variety of residual plots for the CH_4 gas adsorption procedure by Ni-MOF/PVA fibrous network. The positive and negative levels of the experiments are equal, according to the plots. It is possible to conclude from scientific experiment design that adsorption procedure dispersions are randomized [28].

The analysis of variance (ANOVA) method was used to investigate the effects of experimental parameters such as temperature, adsorbent, and pressure on CH_4 gas adsorption. As shown in Table 5, the effect of all parameters is remarkable in terms of having low P_{values} (***A, B***, and ***C***) [29]. The amount of gas adsorption in different samples varies depending on the experimental conditions, according to the results of the analysis of variance and the design of experiments. According to the findings, sample ***c*** has the highest adsorption rate. The amount of adsorbent in this sample was chosen as minimum amount. Although increasing the amount of adsorbent increases the amount of adsorption, it appears that using too much adsorbent results in the formation of structures with agglomeration shapes, which reduces its efficiency [30].

Previous research has also looked into the effects of pressure and temperature. As a result, when compared to other samples, the amount of CH_4 gas adsorption in sample ***c*** has increased significantly. The factorial experiment design appears to have a significant impact on the production of samples with the greatest amount of adsorption. Fig. 10 depicts the Pareto chart of the main interaction of experimental parameters. This chart confirms the effects of experimental parameters and their interactions.

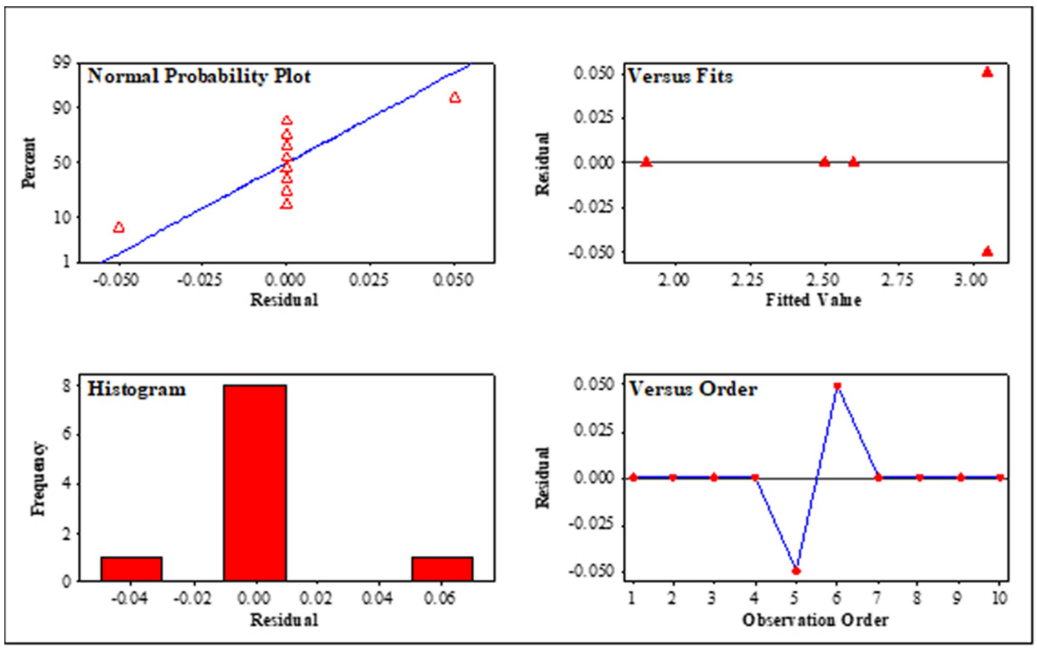

Fig. 9. Normal probability plots for the adsorption of CH_4 gas by a Ni-MOF/PVA fibrous network.

Table 5:

Analyses of variance for CH_4 gas adsorption of Ni-MOF/PVA fibrous network.

Source	DF	Seq SS	Adj SS	Adj MS	P_{value}
A (mg)	1	0.24500	0.032000	0.032000	0.002
B (°C)	1	0.88011	0.047619	0.047619	0.001
C (bar)	1	0.00111	0.032000	0.032000	0.002
A*B	1	0.21778	0.217778	0.217778	0.000
A*C	1	0.21778	0.217778	0.217778	0.03
B*C	1	0.21778	0.217778	0.217778	0.03
R-Sq: 97.24% R-Sq(pred): 99.05% R-Sq(adj): 98.44%					

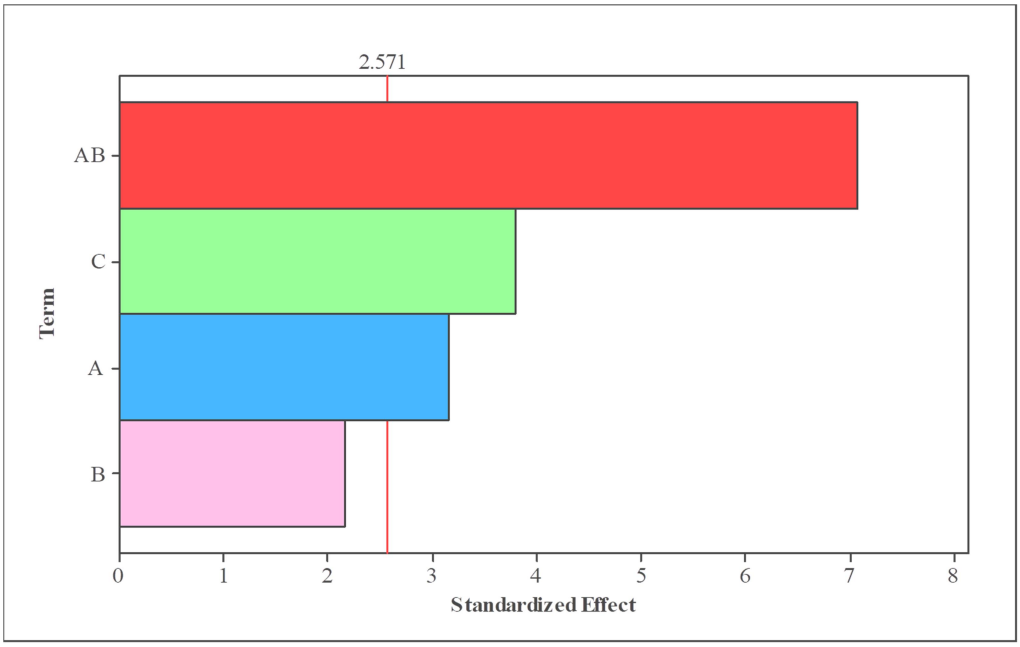

Fig. 10. Pareto charts for CH_4 gas adsorption of Ni-MOF/PVA fibrous network.

4. Conclusion

In this study, the Ni-MOF was immobilized on the surface of PVA using ultrasonic irradiation to increase the specific surface area and stability of the products. FT-IR, XRD, SEM-EDX, TG-DTG etc confirmed the successful synthesis of Ni-MOF/PVA fibrous network. The nanostructures supported on the substrate have a higher surface area and significant porosity than the pure sample, according to BJH method. The surface properties of the final product, as well as the specific surface, allowed this compound to be used as a new option in the field of gas adsorption. Under temperature conditions, the amount of CH_4 gas adsorption by this nanostructure was found up to 3 mmol.

Conflict of interest

The authors declare that they have no conflict of interest.

References

[1] S.H. Hashemi, M. Kaykhaii, A.J. Keikha, E. Mirmoradzehi, G. Sargazi, Application of response surface methodology for optimization of metal–organic framework based pipette-tip solid phase extraction of organic dyes from seawater and their determination with HPLC, BMC chemistry, 13 (2019) 1-10.
[2] S.S. Nadar, L. Vaidya, S. Maurya, V.K. Rathod, Polysaccharide based metal organic frameworks (polysaccharide–MOF): A review, Coordination Chemistry Reviews, 396 (2019) 1-21.
[3] J. Yan, Y. Huang, Y. Yan, X. Zhao, P. Liu, The composition design of MOF-derived Co-Fe bimetallic autocatalysis carbon nanotubes with controllable electromagnetic properties, Composites Part A: Applied Science and Manufacturing, 139 (2020) 106107.
[4] S. Liu, L. Kang, J. Zhang, E. Jung, S. Lee, S.C. Jun, Structural engineering and surface modification of MOF-derived cobalt-based hybrid nanosheets for flexible solid-state supercapacitors, Energy Storage Materials, 32 (2020) 167-177.
[5] M. Shyngys, J. Ren, X. Liang, J. Miao, A. Blocki, S. Beyer, Metal-Organic Framework (MOF)-Based Biomaterials for Tissue Engineering and Regenerative Medicine, Frontiers in Bioengineering and Biotechnology, 9 (2021) 96.
[6] J. Ren, Y. Huang, H. Zhu, B. Zhang, H. Zhu, S. Shen, G. Tan, F. Wu, H. He, S. Lan, Recent progress on MOF-derived carbon materials for energy storage, Carbon Energy, 2 (2020) 176-202.

[7] M.R.R. Kahkha, M. Kaykhaii, G. Sargazi, B.R. Kahkha, Determination of nicotine in saliva, urine and wastewater samples using tantalum metal organic framework pipette tip micro-solid phase extraction, Analytical Methods, 11 (2019) 6168-6175.
[8] S. Kumar, S. Jain, M. Nehra, N. Dilbaghi, G. Marrazza, K.-H. Kim, Green synthesis of metal–organic frameworks: A state-of-the-art review of potential environmental and medical applications, Coordination Chemistry Reviews, 420 (2020) 213407.
[9] X. Liu, M. Zhuo, W. Zhang, M. Gao, X.-H. Liu, B. Sun, J. Wu, One-step ultrasonic synthesis of Co/Ni-catecholates for improved performance in oxygen reduction reaction, Ultrasonics Sonochemistry, 67 (2020) 105179.
[10] F. Akbarzadeh, M. Motaghi, N.P.S. Chauhan, G.J.H. Sargazi, A novel synthesis of new antibacterial nanostructures based on Zn-MOF compound: design, characterization and a high performance application, 6 (2020) e03231.
[11] T. Shahryari, F. Vahidipour, N.P.S. Chauhan, G.J.P.E. Sargazi, Science, Synthesis of a novel Zn-MOF/PVA nanofibrous composite as bioorganic material: Design, systematic study and an efficient arsenic removal, 60 (2020) 2793-2803.
[12] P. Arul, N. Gowthaman, S.A. John, H.N. Lim, Ultrasonic assisted synthesis of size-controlled Cu-metal–organic framework decorated graphene oxide composite: sustainable electrocatalyst for the trace-level determination of nitrite in environmental water samples, ACS omega, 5 (2020) 14242-14253.
[13] J. Bedia, V. Muelas-Ramos, M. Peñas-Garzón, A. Gómez-Avilés, J.J. Rodríguez, C. Belver, A review on the synthesis and characterization of metal organic frameworks for photocatalytic water purification, Catalysts, 9 (2019) 52.
[14] P. Arul, S.-T. Huang, V. Mani, Y.-C. Hu, Ultrasonic synthesis of bismuth-organic framework intercalated carbon nanofibers: A dual electrocatalyst for trace-level monitoring of nitro hazards, Electrochimica Acta, 381 (2021) 138280.
[15] M. Stanisz, Ł. Klapiszewski, T. Jesionowski, Recent advances in the fabrication and application of biopolymer-based micro-and nanostructures: A comprehensive review, Chemical Engineering Journal, 397 (2020) 125409.
[16] G. Fadillah, O.A. Saputra, T.A. Saleh, Trends in polymers functionalized nanostructures for analysis of environmental pollutants, Trends in Environmental Analytical Chemistry, 26 (2020) e00084.
[17] M. Zeraati, V. Alizadeh, S. Chupradit, N.P.S. Chauhan, G.J.J.o.M.S. Sargazi, Green Synthesis and Mechanism Analysis of a New Metal-Organic Framework Constructed from Al (III) and 3, 4-Dihydroxycinnamic Acid Extracted from Satureja hortensis and its anticancerous activities, (2021) 131712.
[18] G. Sargazi, D. Afzali, A. Mostafavi, H. Kazemian, A novel composite derived from a metal organic framework immobilized within electrospun nanofibrous polymers: An efficient methane adsorbent, Applied Organometallic Chemistry, 34 (2020) e5448.
[19] H. Wang, B. Yuan, R. Hao, Y. Zhao, X. Wang, A critical review on the method of simultaneous removal of multi-air-pollutant in flue gas, Chemical Engineering Journal, 378 (2019) 122155.
[20] I. Klewiah, D.S. Berawala, H.C.A. Walker, P.Ø. Andersen, P.H. Nadeau, Review of experimental sorption studies of CO2 and CH4 in shales, Journal of Natural Gas Science and Engineering, 73 (2020) 103045.
[21] X.-Y. Li, B.-B. Ge, J. Yan, Y.-Y. Lu, D.-L. Zhong, P. Englezos, B.-Y. Zhang, Review on Hydrate-Based CH4 Separation from Low-Concentration Coalbed Methane in China, Energy & Fuels, 35 (2021) 8494-8509.
[22] G. Sargazi, D. Afzali, A. Mostafavi, A. Shadman, B. Rezaee, P. Zarrintaj, M.R. Saeb, S. Ramakrishna, M. Mozafari, Chitosan/polyvinyl alcohol nanofibrous membranes: towards green super-adsorbents for toxic gases, Heliyon, 5 (2019) e01527.

[23] R. Abazari, A.R. Mahjoub, S. Molaie, F. Ghaffarifar, E. Ghasemi, A.M. Slawin, C.L. Carpenter-Warren, The effect of different parameters under ultrasound irradiation for synthesis of new nanostructured Fe3O4@ bio-MOF as an efficient anti-leishmanial in vitro and in vivo conditions, Ultrasonics sonochemistry, 43 (2018) 248-261.
[24] S. Gao, Y. Sui, F. Wei, J. Qi, Q. Meng, Y. He, Facile synthesis of cuboid Ni-MOF for high-performance supercapacitors, Journal of materials science, 53 (2018) 6807-6818.
[25] L. Jin, J. Ye, Y. Wang, X. Qian, M. Dong, Electrospinning synthesis of ZIF-67/PAN fibrous membrane with high-capacity adsorption for malachite green, Fibers and Polymers, 20 (2019) 2070-2077.
[26] Y. Qiao, Q. Liu, S. Lu, G. Chen, S. Gao, W. Lu, X. Sun, High-performance non-enzymatic glucose detection: using a conductive Ni-MOF as an electrocatalyst, Journal of Materials Chemistry B, 8 (2020) 5411-5415.
[27] Y. Chen, D. Ni, X. Yang, C. Liu, J. Yin, K. Cai, Microwave-assisted synthesis of honeycomblike hierarchical spherical Zn-doped Ni-MOF as a high-performance battery-type supercapacitor electrode material, Electrochimica Acta, 278 (2018) 114-123.
[28] S. Zhang, Z. Fan, J. Li, S. Wen, S. Paddea, L. Lu, S. Li, Experimental Characterisation and Numerical Modelling of Residual Stresses in a Nuclear Safe-End Dissimilar Metal Weld Joint, Metals, 11 (2021) 1298.
[29] A. Henrique, M. Karimi, J.A. Silva, A.E. Rodrigues, Analyses of adsorption behavior of CO2, CH4, and N2 on different types of BETA zeolites, Chemical Engineering & Technology, 42 (2019) 327-342.
[30] V. Ghalandari, H. Hashemipour, H. Bagheri, Experimental and modeling investigation of adsorption equilibrium of CH4, CO2, and N2 on activated carbon and prediction of multi-component adsorption equilibrium, Fluid Phase Equilibria, 508 (2020) 112433.